Characterization of amphoteric bentonite-loaded magnetic biochar and its adsorption properties for Cu^{2+} and tetracycline

Hongyan Deng[1,*], Haixia He[1,*], Wenbin Li[1], Touqeer Abbas[2] and Zhifeng Liu[3]

[1] College of Environmental Science and Engineering, China West Normal University, Nanchong, China
[2] Key Laboratory of Environment Remediation and Ecological Health, Ministry of Education, Zhejiang University, Zhejiang, China
[3] Qinba Mountains of Bio-Resource Collaborative Innovation Center of Southern Shaanxi Province, Hanzhong, China
* These authors contributed equally to this work.

ABSTRACT

To realize simultaneous adsorption of heavy metal and antibiotic pollutants by a BC-based recyclable material, Fe_3O_4 magnetic biochar (MBC) was prepared by co-precipitation method. Then different ratios of dodecyl dimethyl betaine (BS-12)-modified bentonite (BS-B) were loaded on the surfaces of biochar (BC) and MBC to prepare BS-B-loaded BC and MBC composites, called BS-B/BC and BS-B/MBC, respectively. The physicochemical and structural properties of the composites were characterized by scanning electron microscopy, Fourier transform infrared spectrometry, thermogravimetric analysis, specific surface area (S_{BET}) analysis, and vibrating sample magnetometry, and the adsorption efficiencies of BS-B/BC and BS-B/MBC to Cu^{2+} and tetracycline (TC) were studied. The following results were obtained. (1) Compared with BS-B/BC, BS-B/MBC had decreased pH and cation exchange capacity (CEC) and increased S_{BET}. The pH, CEC, and S_{BET} of BS-B/BC and BS-B/MBC decreased with the increase in the BS-12 proportion of BS-B. The surface of BS-B/MBC became rough after Fe_3O_4 loading. (2) The residual rate of BS-B/MBC was higher than that of BS-B/BC after high-temperature combustion, and the residual rate decreased with the increase in the BS-12 proportion of BS-B. The 2D infrared spectra showed that Fe_3O_4 and BS-12 were modified on the surface of BS-B/MBC. MBC and BS-B/MBC had splendid magnetism and could be separated by external magnetic field. (3) Compared with unmagnetized ones, the adsorption effects of Cu^{2+} and TC on different BS-B/MBCs improved, and the average adsorption rate reached the largest value of 91.92% and 97.76%, respectively. Cu^{2+} and TC adsorptions were spontaneous, endothermic, and entropy-increasing processes. The pH and S_{BET} of the material had a great influence on Cu^{2+} and TC adsorptions, respectively, than CEC.

Submitted 1 November 2021
Accepted 8 February 2022
Published 1 March 2022

Corresponding author
Wenbin Li, lwb062@cwnu.edu.cn

Academic editor
Monika Mortimer

Additional Information and Declarations can be found on page 17

DOI **10.7717/peerj.13030**

Subjects Environmental Contamination and Remediation, Environmental Impacts, Green Chemistry
Keywords Magnetized biochar, Bentonite, Dodecyl dimethyl betaine, Surface characteristics, Adsorption capacity

INTRODUCTION

Heavy metal and antibiotics in livestock farm wastewater has become one of the focuses of research (*Nyamukamba et al., 2019*). The metabolites of heavy metals and antibiotics have strong persistence, difficult degradation, and easy accumulation; can exist in water and soil environment for a long time; and eventually threaten human health through the food chain (*Khan et al., 2015*; *Min et al., 2018*). Therefore, screening remediation materials with high adsorption capacity and good recycling performance for heavy metal and antibiotic have great importance for the pollution control of livestock and poultry breeding and the sustainable development of agriculture.

The remediation methods for water pollution include physical, chemical, and biological remediation (*Mazurkiewicz et al., 2020*; *Zulfiqar et al., 2021*; *Kumar et al., 2021*). Among which, material adsorption has become a hot spot in pollution remediation research because of its simple operation, low cost, and obvious effect (*Fu et al., 2019*; *Isakovski et al., 2020*; *Kumar et al., 2021*). Many repair materials, such as biochar (BC) (*Ahmad et al., 2014*; *He et al., 2019*), clay minerals (*Beraa et al., 2016*), and agricultural and forestry wastes (*Garg et al., 2021*), have been studied. The surface of BC contains a large number of negatively charged functional groups, which greatly adsorb heavy metals and organic pollutants in water environment (*Mohan et al., 2014*; *Yang et al., 2016*). The adsorption capacities of straw BC for Cd^{2+} and methylene blue are 30.19 and 46.60 mg/g, respectively (*Park et al., 2016*; *Li et al., 2016a*). *Feng et al. (2020)* found that the adsorption capacity of bamboo–willow BC for oxytetracycline and sulfaethoxazole are 11.98 and 10.12 mg/g, respectively. The adsorption isotherm models of BC for phenol and tannic acid are multilayer and monolayer, respectively (*Lawal et al., 2021*). BC materials have good adsorption effect on pollutants but are difficult to separate in aqueous solution. Some researchers loaded magnetic particles on the surface of BC by Fe_3O_4, and realized the separation of BC material in solution by magnetic force. Then, the pollutants absorbed on the magnetic biochar (MBC) are eluted for the recycling of the MBC (*Yan et al., 2015*; *Wang et al., 2020*). Studies have shown that MBC can form a weak magnetic field around them to improve the metabolic capacity of microorganisms, accelerate the decomposition of pollutants, and thus reduce the concentrations of pollutants (*Kastner, Mani & Juneja, 2015*; *Kyung-Won et al., 2016*).

Bentonite (B) has strong adsorption capacity, ion exchange capacity and expansibility as a good pollution remediation material (*Said & Goda, 2021*). Current research on organic B focuses on its modification using surfactants to enhance its adsorption and fixation of pollutants. Amphoteric surface modifiers have hydrophilic positive and negative charges and hydrophobic carbon chains, which can adsorb organic and heavy metal pollution, simultaneously. Therefore, using amphoteric surface modifiers to modify B can simultaneously improve the adsorption performance of B to organic matter and heavy

metals (*Li et al., 2016b*). The adsorption amounts of Cd^{2+} and phenol on Lou soil modified by amphoteric surface modifier (BS-12) were 1.3–1.8 and 4.0–8.3 times higher than those on unmodified soil sample, respectively (*Meng, Zhang & Wang, 2007*). The magnetization method realizes the secondary utilization of BC but does not improve its adsorption capacity for pollutants (*He et al., 2019*; *Wang et al., 2020*). Therefore, loading amphoteric B on MBC can greatly improve the adsorption capacity of the MBC to various pollutants and realize the recycling of the material synchronously.

Alternanthera philoxeroides BC and BS-12-modified B (BS-B) were prepared by oxygen-limiting high-temperature pyrolysis and wet method, respectively, and MBC was prepared by co-precipitation method to verify the absorption effect of BS-B-loaded MBC (BS-B/MBC) on heavy metal and antibiotic pollution. Then, BS-B-loaded BC (BS-B/BC) and BS-B/MBC were prepared by separately loading BS-B on the surfaces of BC and MBC, and the properties and structure of the composite materials were characterized.
In addition, the isothermal adsorption and thermodynamic characteristics of Cu^{2+} and tetracycline (TC) on the composite materials were studied to provide a reference for the application of BC-based composite materials in sewage treatment.

MATERIALS AND METHODS

Materials

Dodecyl dimethyl betaine was used as the amphoteric modifier, which abbreviated as BS-12 (AR; produced by Tianjin Xingguang Reagent Factory, Tianjin City, China). The B used was sodium B, which purchased from Henan Xinyang Bentonite Produce Company and purified by washing method before use (*Shah et al., 2018*). The basic physicochemical properties of the purified B are: cation exchange capacity (CEC) is 1,000.33 mmol/kg, pH is 9.59, and total organic carbon (TOC) is 4.98 g/kg. $FeCl_3{\cdot}6H_2O$, $FeSO_4{\cdot}7H_2O$ and NaOH were all purchased from Chengdu Kelong Chemical Reagent Factory, Chengdu City, Sichuan Province, China. TC was purchased from Sigma (St. Louis, MO, USA) and had a purity of 99.9%. Cu^{2+} solution was used as pollutant, and the solution was prepared by using $CuSO_4{\cdot}5H_2O$ (analytical reagent) purchased from Chengdu Kelon Chemical Reagent Factory. Figures 1A and 1B show the structural formula of BS-12 and TC, respectively.

BS-B was prepared by wet method (*Li et al., 2016b*). BS-12 solution was added into 10 g of purified B (the mass ratio between solution and soil was 10:1), then reacted for 6 h at 40 °C; Centrifuged at 4,800 r/min for 10 min, washed 3 times with deionized water (dH_2O), dried, grinded and sieved through 60-mesh nylon sieve to obtain BS-B.
The amount use of BS-12 modifier was defined by Eq. (1):

$$W = m \times \mathrm{CEC} \times \mathrm{M} \times 10^{-6} \times R_{\mathrm{BS}}/C_{\mathrm{BS}} \quad (1)$$

where W_{BS} stands for the mass (g) of BS-12; m stands for the mass (g) of bentonite; CEC stands for the cation exchange capacity of the bentonite (mmol/kg); M_{BS} stands for the relative molar mass of BS-12 (g/mol); R_{BS} stands for the modification ratio (50% or 100%) of BS-12; C_{BS} stands for the content (mass fraction) of BS-12.

A. philoxeroides was washed with dH_2O, dried to constant weight under 60 °C, grinded and sieved through a 200-mesh nylon sieve, and fired for 8 h under 400 °C by

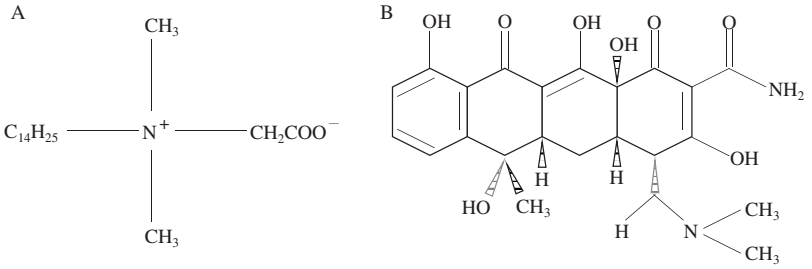

Figure 1 **Structural formulas of BS-12 (A) and TC (B).** Full-size DOI: 10.7717/peerj.13030/fig-1

oxygen-limiting high-temperature pyrolysis to obtain BC. Co-precipitation method was used to prepare MBC (*He et al., 2019*). In this method, 20.00 g BC was dispersed in 2.0 L dH_2O and stirred for 30 min. Under strictly anaerobic conditions, 0.4 M $FeCl_3{\cdot}6H_2O$ and 0.2 M $FeSO_4{\cdot}7H_2O$ were successively added to 60 °C water, fully stirred for 2 h, and heated to 75 °C. The pH was adjusted to 10 with 5 mol/L NaOH solution and the MBC was separated by magnets after continuous stirring for 1 h and natural cooling. MBC was obtained after washing several times with dH_2O. MBC was dried at 60 °C and then passed through a 60-mesh sieve. A wet process was used to prepare BS-B/BC and BS-B/MBC. In this process, 100 g BC or MBC was slowly added to 1.0 L dH_2O, and BS-B was added again. After stirring at 40 °C for 3 h, the samples were separated, washed by dH_2O thrice and dried at 60 °C. Then, BS-B/BC and BS-B/MBC were dried at 60 °C for 12 h and passed through a 60-mesh sieve.

Experimental design

BS-B samples with BS-12 proportions of 0%, 50%, and 100% were prepared and named as B (bentonite only), 50BS-B, and 100BS-B, respectively. BC and MBC were used as the control (CK). BC, B/BC, 50BS-B/BC, 100BS-B/BC, MBC, B/MBC, 50BS-B/MBC, and 100BS-B/MBC (8 samples in total) were analyzed for the pH, CEC, and Brunaer–Emmett–Telle specific surface area (S_{BET}), and characterized by scanning electron microscopy (SEM), thermogravimetry (TG), Fourier transform infrared (FT-IR) spectroscopy, and vibration sample magnetometry (VSM).

The pre-experiment of Cu^{2+} adsorption showed that the adsorption isotherm began to turn at 300–400 mg/L, so the Cu^{2+} concentration in isothermal adsorption experiment was set to 0, 20, 50, 100, 150, 200, 300, 400, and 500 mg/L for a total of nine concentration gradients. The concentration of tetracycline was set to 0, 2, 5, 10, 20, 40, 60, 80, and 100 mg/L nine concentration gradients by their pre-experiment. Three replicates were set for each treatment.

Experimental methods

pH value was determined using a HQ411D table pH meter (Hash Company, Vancouver, WA, USA; refer to the test method of soil sample, solid–liquid ratio was 1:5). CEC was determined by sodium acetate–ammonium acetate method. S_{BET} was analyzed by by multi-point BET method using a V-Sorb2800P analyzer. SEM was performed using a Japanese Hitachi S-4800 scanning electron microscope. TG was performed using a

STA449F3 synchronous thermal analyzer (NETZSCH) under the following conditions: temperature range 25–900 °C; sample quality, 10–15 mg; heating rate, 10 °C/min; N_2 atmosphere. FT-IR analysis was performed on a Nicolet 5DX type Fourier transform infrared spectrometer, and the 2D FTIR spectra were analyzed by 2DShige software. Magnetic curves were determined by Lakeshore 665 VSM method.

Nine samples (0.5000 g) of each composite material were separately packed in 50 mL plastic centrifuge tubes, added with 20 mL of Cu^{2+} (TC) solutions under different concentration gradients, shaken at room temperature for 12 h (200 r/min), and centrifuged at 4,800 r/min for 15 min. The supernatant was collected to determine the Cu^{2+} (TC) concentration, and the actual adsorption amount of the test material was calculated by subtraction (*Zhang et al., 2020*; *Zou et al., 2020*). The experiments were carried out at 20 and 40 °C respectively for calculating the thermodynamic parameters of Cu^{2+} and TC adsorptions. The Cu^{2+} content was determined *via* flame atomic absorption spectrophotometry, and background absorption was corrected through the Zeeman effect. The TC concentration was determined by SP-2100 UV-VIS spectrophotometer at 365 nm. The above measurements were all inserted into standard solutions for analysis quality control.

Data processing

The equilibrium adsorption amount of Cu^{2+} and TC was calculated using Eq. (2):

$$q = \frac{V \times (C_0 - C_e)}{W_0} \tag{2}$$

where C_0 (mmol/L) and C_e (mmol/L) are the initial and equilibrium concentrations of Cu^{2+} (or TC) in the solution, respectively. V (mL) is the volume of Cu^{2+} (or TC) solution added. W_0 (g) is the weight of the tested material. q (mmol/kg) is the equilibrium adsorption amount of Cu^{2+} (or TC) on the tested material.

The adsorption rate AR (%) of Cu^{2+} and TC was calculated using Eq. (3):

$$AR = \frac{100 \times (C_0 - C_e)}{C_0} \tag{3}$$

The Langmuir isotherm was selected on the basis of the adsorption isotherm trend and the isothermal equation Eq. (4) is as follows (*Zhang et al., 2020*):

$$q = \frac{q_m b C_e}{1 + b C_e} \tag{4}$$

where q_m indicates the maximum adsorption amount of Cu^{2+} (or TC) on the different materials, mmol/kg; b represents the apparent equilibrium constant of the Cu^{2+} (or TC) adsorption, which can be used to measure the affinity of adsorption.

Parameter b in the Langmuir model is equivalent to the apparent adsorption constant of equilibrium constant, and the thermodynamic parameter calculated by $b = K$ or K_a is called the apparent thermodynamic parameters; Eqs. (5)–(7) are as follows (*Zhao et al., 2021*):

$$\Delta G = -RT \ln K \tag{5}$$

$$\Delta H = R\left(\frac{T_1 \cdot T_2}{T_2 - T_1}\right) \cdot \ln\left(\frac{K_a, T_2}{K_a, T_1}\right) \tag{6}$$

$$\Delta S = \frac{\Delta H - \Delta G}{T} \tag{7}$$

where ΔG is the standard free energy change (kJ/mol), R is a constant (8.3145 J/mol/K), T is the adsorption temperature (T_1 = 293.16 K, T_2 = 313.6 K), ΔH is the enthalpy of adsorption process (kJ/mol), and ΔS is the entropy change of adsorption process (J/mol/K).

CurveExpert 1.4 fitting software was used in isothermal fitting, and SigmaPlot 10.0 software was adopted to improve data plotting. SPSS 16.0 statistical analysis software was used to process the experimental data for variance and correlation analysis (*Li et al., 2020*). SigmaPlot 10.0 software was adopted to improve data plotting. The data were expressed as the means with standard deviation, and different letters indicate significant differences among various amendments (*Lopez et al., 2012*). Analysis of variance was performed to determine the effects of amendments, followed by Tukey's honestly significant difference test. Differences of $p < 0.05$ were considered significant (*Ana et al., 2013*).

RESULTS

Basic physicochemical properties of the tested materials

Figure 2 shows the physicochemical characteristics of each test material. The pH and CEC of BC increased when B was loaded but decreased when BS-B was loaded, and the amplitude decreased with the increase in the BS-12 proportion of BS-B. S_{BET} decreased when BC was loaded with B and BS-B, and further decreased with the increase in the modification ratio of BS-12 on BS-B. B/BC had a slight increase in pH and a higher increase in CEC, which may be caused by the similar pH and larger CEC of B than those of BC. BS-12 on BS-B can neutralize the alkalinity of B, and the long carbon chains of BS-12 can cover the surface of B and thus reduce the CEC of BS-B. Therefore, when BC was loaded with BS-B, the pH and CEC of BS-B/BC materials decreased with the increase in the modification ratio of BS-12. Moreover, when BC was loaded with BS-B, the interlayer or surface pores of BC were covered by BS-B, which increased the average particle size of BS-B/BC and resulted in the decrease in S_{BET}. Compared with the unmagnetized ones, the magnetized materials had slightly reduced pH and CEC and remarkably increased S_{BET} because the increase in Fe_3O_4 particles increased the roughness of a material's surface and then increased its surface area (*He et al., 2019*).

SEM images of the test materials

The SEM image of the surface morphology of each test material is shown in Fig. 3. BC had a smooth surface and a regular pore structure. When BC surface was loaded with B, the surface of B/BC became rough, a few number of B particles were attached to the surface of BC, and some pores were also filled with B particles. When BC was loaded with

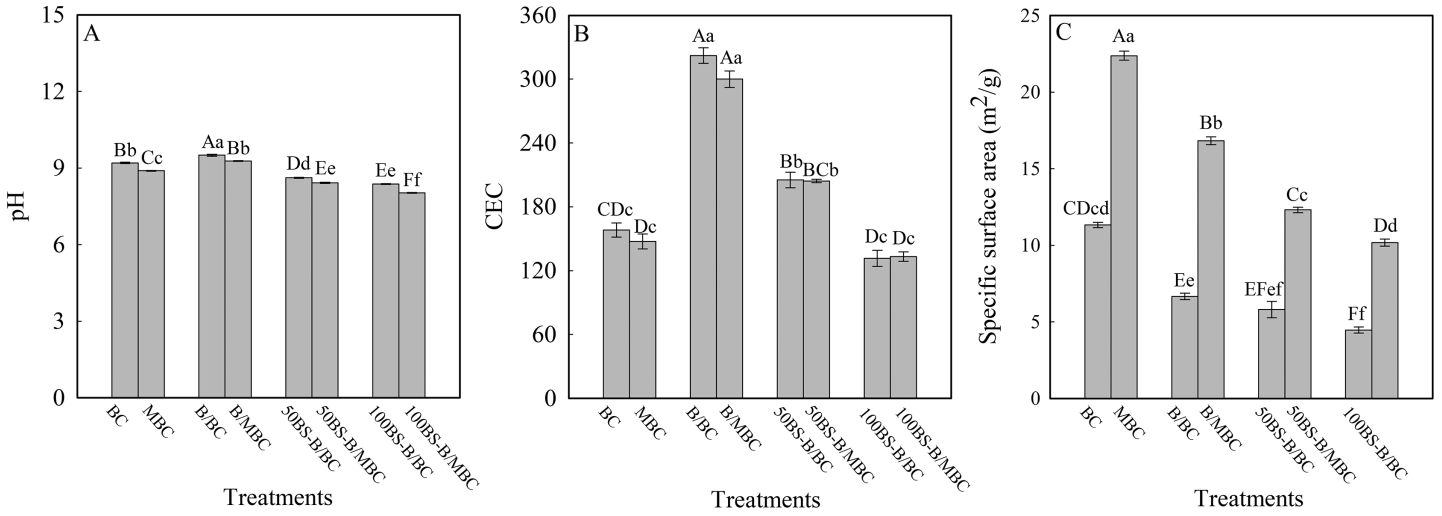

Figure 2 Physical and chemical characteristics of the test materials. (A–C) pH, CEC, and specific surface area, respectively. BC and MBC stand for original biochar and magnetic biochar, respectively. B/BC, 50BS-B/BC, and 50BS-B/BC were 0%, 50%, and 100% BS-12 modified bentonite loaded BC. B/MBC, 50BS-B/MBC, and 50BS-B/MBC represent 0%, 50%, and 100% BS-12 modified bentonite loaded MBC. The same as other figures. The different uppercase and lowercase letters indicate significant difference among treatments at p = 0.0 1 and p = 0.05 level, respectively.
Full-size DOI: 10.7717/peerj.13030/fig-2

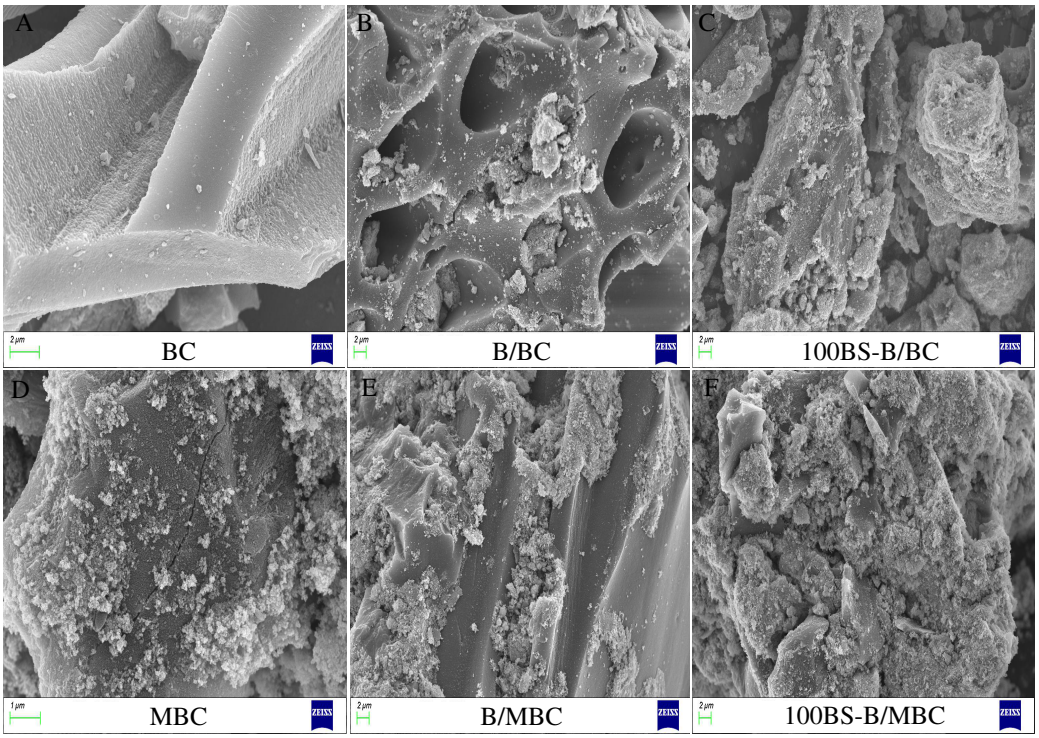

Figure 3 SEM images of test materials. (A–F) BC, B/BC, 100BS-B/BC, MBC, B/MBC, and 100BS-B/MBC, respectively.
Full-size DOI: 10.7717/peerj.13030/fig-3

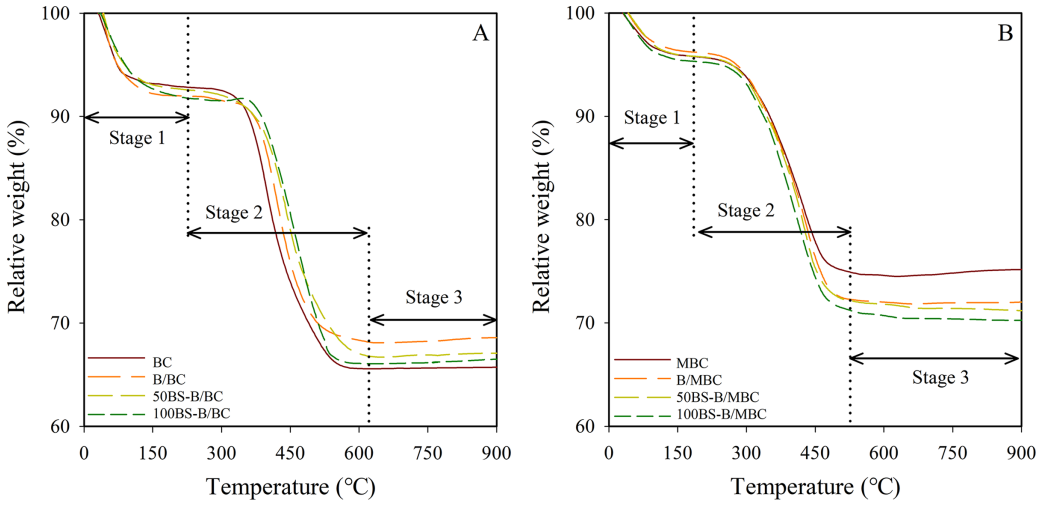

Figure 4 TG curves of test materials. (A–B) Unmagnetized and magnetized materials, respectively.
Full-size DOI: 10.7717/peerj.13030/fig-4

100BS-B, the surface smoothness of 100BS-B/BC increased, because the hydrophobic long carbon chain of BS-12 could form a layer of organic phase on the surface of 100BS-B, which could decreased the surface roughness (*Zhang et al., 2020*). When each composite material was loaded with Fe_3O_4, its surface became rough compared with the unmagnetized ones. A large number of Fe_3O_4 particles were attached to the surface of the material, and some pores were also filled with Fe_3O_4 particles. The results show that Fe_3O_4 had a large effect on the surface morphology of the magnetic material, and the iron oxide particles were dispersed on the carbon matrix, which increased the S_{BET} (*Xin et al., 2017*).

TG analysis of the tested materials

The TG curves of the different materials are shown in Fig. 4. The test materials had different degrees of weight loss after high-temperature pyrolysis (900 °C), and the weight loss rates of the materials were greater after magnetization. The weight loss of the test materials is in the order: BC > 100BS-B/BC > 50BS-B/BC > B/BC, 100BS-B/MBC > 50BS-B/MBC > B/MBC > MBC. As the modification ratio of BS-12 increased, the weight loss rate of BS-B/BC and BS-B/MBC materials gradually increased, mainly because the surface active agent BS-12 was decomposable organic matter (*He et al., 2019*). Change in the TG curve showed three stages at the temperatures of 0–250 °C, 250–600 °C, and 600–900 °C, which represent the material water loss, organic matter decomposition, and crystal layer collapse, respectively.

Table 1 shows the weight loss rate and differential thermogravimetric (DTG, mass change rate with time, %/min) peak temperature of each material in the three stages of the TG curve. The DTG peak temperatures of the test materials were kept between 67 °C and 81 °C in the water loss stage (Stage 1). The water loss rates of the test materials are in the order: 100BS-B/BC (8.26%) > B/BC (8.07%) > 50BS-B/BC (7.51%) > BC (6.68%) >

Table 1 TG (%) and DTG (%/min) curves of the test materials. BC and MBC stand for original biochar and magnetic biochar, respectively. B/BC, 50BS-B/BC, and 50BS-B/BC were 0%, 50%, and 100% BS-12 modified bentonite loaded BC. B/MBC, 50BS-B/MBC, and 50BS-B/MBC represent 0%, 50%, and 100% BS-12 modified bentonite loaded MBC. The same information applies to the other tables.

Treatments	Dehydration Stage 1 (<250 °C)		Organic carbon decomposition Stage 2 (250–600 °C)		Crystal layer collapse Stage 3 (>600 °C)	Residual rate (%)
	Water loss rate (%)	Peak temperature (°C)	Carbon loss rate (%)	Peak temperature (°C)	Peak temperature (°C)	
BC	6.68	67.13	11.6	403.49	618.98	65.71
B/BC	8.07	68.34	15.1	444.69	633.35	68.61
50BS-B/BC	7.51	69.51	18.04	481.68	692.78	67.28
100BS-B/BC	8.26	67.25	23.48	525.85	750.44	66.63
MBC	4.59	68.16	15.96	436.72	640.11	75.19
B/MBC	4.17	79.82	19.2	448.31	651.61	72.01
50BS-B/MBC	4.74	80.67	20.07	451.87	652.43	71.18
100BS-B/MBC	5.02	70.48	21.17	455.23	642.39	70.24

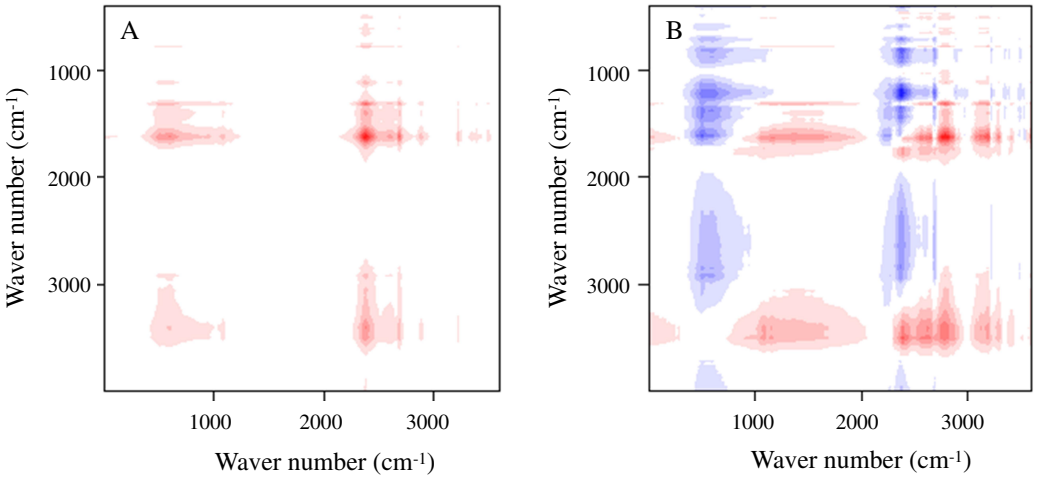

Figure 5 2D infrared spectra of the test materials. (A–B) Synchronous and asynchronous correlation diagram, respectively. Full-size DOI: 10.7717/peerj.13030/fig-5

100BS-B/MBC (5.02%) > 50BS-B/MBC (4.74%) > MBC (4.59%) > B/MBC (4.17%). In the organic carbon decomposition stage (Stage 2), the DTG peak temperatures of the test materials was kept between 400 °C and 530 °C. The carbon loss rate of BC was only 11.6%, whereas the carbon loss rates of the other test materials were in the range of 15.1–23.48%. Carbon loss rate increased with the increase in the modification ratio of BS-12. Almost no weight loss was observed in all the tested materials in the crystal layer collapse stage (Stage 3), and the DTG peak temperatures were in the range of 550–900 °C. This part of weight loss change is only related to the composition and structure of the material itself and has nothing to do with the organic modification.

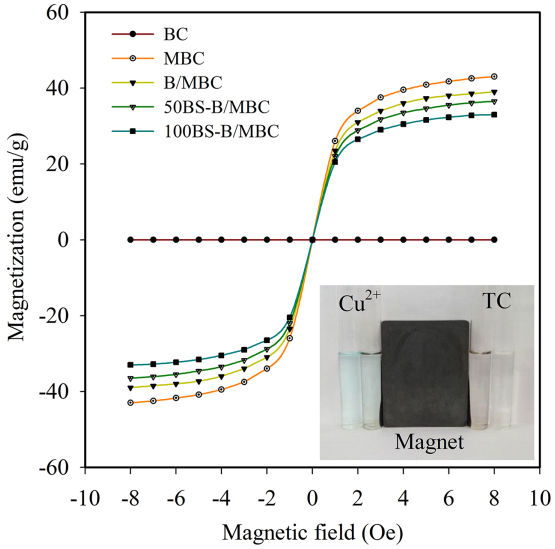

Figure 6 **Hysteresis curves and magnetic effects of the test materials.**
Full-size DOI: 10.7717/peerj.13030/fig-6

FTIR and magnetic characteristics of the test materials

The 2D infrared spectra of the test materials are shown in Fig. 5A (synchronous correlation diagram) and Fig. 5B (asynchronous correlation diagram), The red and blue marks in the figures indicate positive and negative reactions, respectively. The test materials presented a strong characteristic absorption peak of Fe–O bond near 659–695 cm^{-1}, which indicates that Fe_3O_4 was modified to the surface of BC materials. The peak in the vicinity of 990 cm^{-1} is the O–H surface modal vibration absorption on the carboxyl group, which is related to the carboxyl group and the amine group in the BS-12 molecule. This result indicates that BS-12 bound to MBC. A characteristic absorption peak containing the C=O functional group appeared at 1,600 cm^{-1}, and the deformation vibration characteristic absorption peak of the C–H bond appeared near 2,920 cm^{-1}. The absorption peak at 3,438 cm^{-1} was produced by the stretching vibration of the –OH bond. These results confirm that BS-B and Fe_3O_4 were loaded on the BC surface.

The results of the hysteresis curve in Fig. 6 show that MBC and BS-B/MBC have good magnetic separation performance. The saturation magnetization of MBC was 43 emu/g. After BS-B loading, the magnetism of BS-B/MBC decreased slightly with the increase in BS-12 modification on BS-B. BS-B/MBC could still be separated by applying a magnetic field, which was of great importance for the recycling of BS-B/MBC materials.

Isothermal adsorption and thermodynamic parameters of Cu^{2+}

The Cu^{2+} adsorption isotherms and adsorption rates of the test materials are shown in Fig. 7. The adsorption capacity of Cu^{2+} increased with the increase in equilibrium concentration, and the adsorption isotherm of the test materials to Cu^{2+} all conformed to the Langmuir model. The Cu^{2+} adsorption capacity of BC increased obviously after B

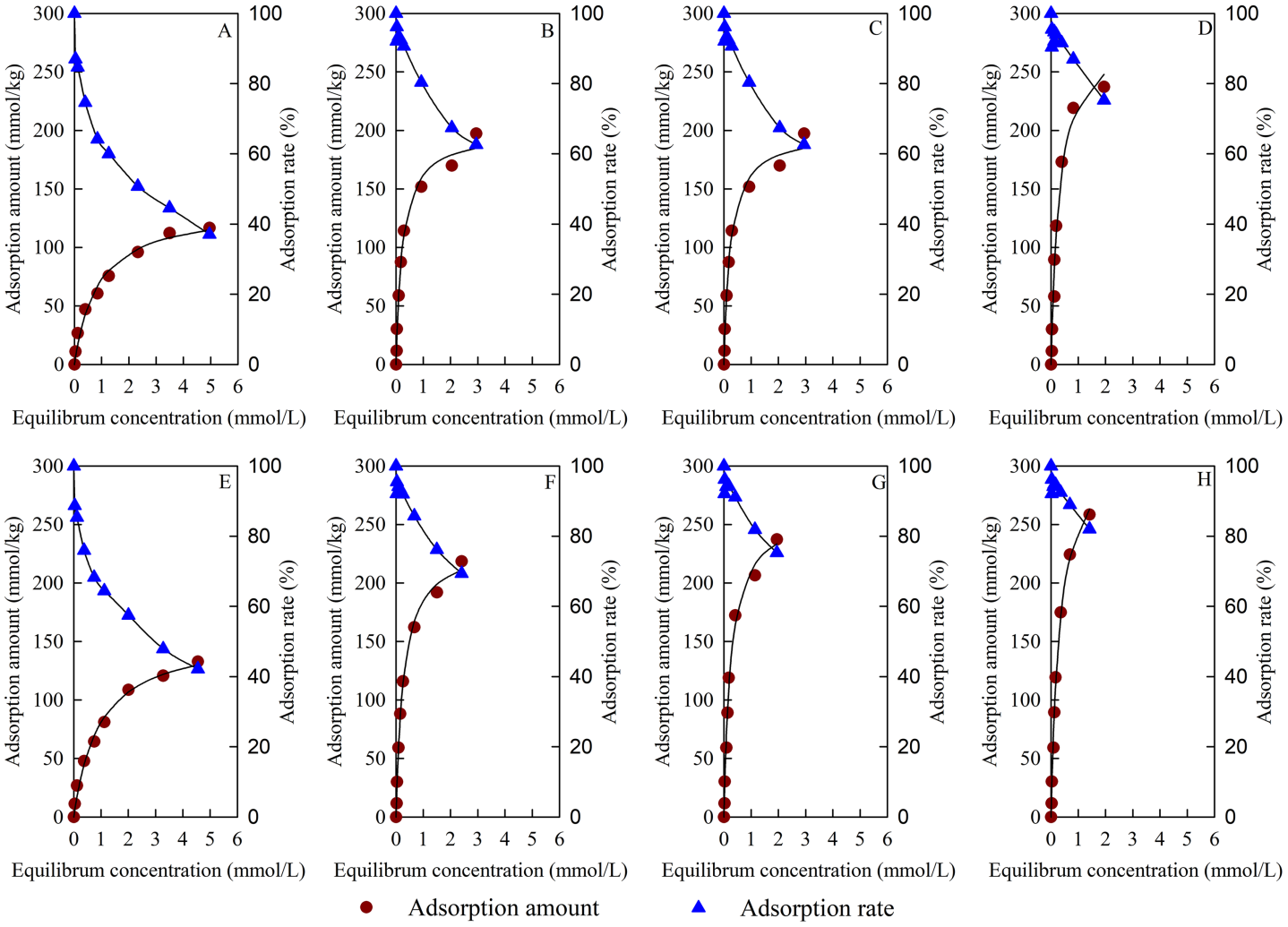

Figure 7 Adsorption isotherm and adsorption rate of Cu^{2+}. (A–H) BC, B/BC, 50BS-B/BC, 100BS-B/BC, MBC, B/MBC, 50BS-B/MBC, and 100BS-B/MBC, respectively.
Full-size DOI: 10.7717/peerj.13030/fig-7

loading. The Cu^{2+} adsorption capacity of BS-B/MBC increased with the increase in the modification ratio of BS-12 on BS-B. Compared with the unmagnetized ones, the magnetized materials had increased Cu^{2+} adsorption capacity.

Table 2 shows the fitting parameters and thermodynamic parameters of Cu^{2+} adsorption by Langmuir model. The correlation coefficient reached an extremely significant level ($p < 0.01$). The maximum adsorption capacity (q_m) of different materials changed from 135.07 mmol/kg to 322.00 mmol/kg. Compared with unmagnetized ones, the magnetized materials had higher q_m for Cu^{2+}. 100BS-B/MBC had the best adsorption effect on Cu^{2+}; its q_m reached 322.00 mmol/kg, and its average adsorption rate (AR_e) was 91.92%. The values of the adsorption constant (b) of magnetized materials for Cu^{2+} were smaller than those of unmagnetized ones, which indicates that

Table 2 Langmuir fitting parameters and thermodynamic parameters for Cu^{2+} adsorption.

Treatments	Fitting parameters				Average adsorption rate (%)	Thermodynamic parameters			
	Correlation coefficient/*r*	Standard deviation/*S*	q_m (mmol/kg)	*b*		ΔG_{20} (kJ/mol)	ΔG_{40} (kJ/mol)	ΔH (kJ/mol)	ΔS (J/mol/K)
BC	0.9923**	5.70	135.07	1.16	62.87	−17.13	−18.62	4.76	74.68
B/BC	0.9948**	7.78	199.80	4.22	84.42	−20.25	−21.84	3.07	79.55
50BS-B/BC	0.9905**	12.02	240.43	4.10	88.21	−20.15	−21.77	3.49	80.67
100BS-B/BC	0.9897**	13.59	286.31	3.32	90.08	−19.70	−21.22	2.64	76.21
MBC	0.9949**	5.20	157.18	1.06	66.29	−16.75	−18.43	7.89	84.03
B/MBC	0.9978**	5.60	234.77	3.67	87.31	−19.76	−21.57	6.72	90.33
50BS-B/MBC	0.9954**	8.89	264.49	3.92	89.93	−20.04	−21.61	3.00	78.60
100BS-B/MBC	0.9968**	8.03	322.00	3.15	91.92	−19.52	−21.07	3.23	77.61

Note:
** The correlation coefficient is significant at $p = 0.01$ level ($r = 0.798$ when the degree of freedom $f = 7$ and the level of significance $p = 0.01$).

magnetization reduced the adsorption affinity of BC materials to Cu^{2+}. This outcome might be due to the fact that Fe_3O_4 particles block the pores of BC materials, which results in the reduction of exchangeable cation sites on the surface. The *b* values of BS-B/BC and BS-B/MBC were larger than those of BC and MBC, which indicates that the adsorption affinity to Cu^{2+} became greater after BS-B loading. B had a larger CEC and could have an ion exchange reaction with more Cu^{2+}, and B loading could promote Cu^{2+} adsorption. The value of *b* was the largest when BC was loaded with B but decreased with the increasing in BS-12 modification rate on BS-B when BC was loaded with BS-B. This result indicates that BS-12 formed an organic coating on the surface of BC and reduced its adsorption affinity for Cu^{2+}.

At 20 and 40 °C, the Gibbs free energy (ΔG) values for the Cu^{2+} adsorption of each test material were less than 0, which indicates that the adsorption was a spontaneous reaction. The adsorption enthalpy change (ΔH) of each tested material to Cu^{2+} was greater than 0, which indicates that the adsorption was an endothermic reaction, and increasing temperature was conducive to the occurrence of adsorption. The entropy change (ΔS) of each test material was greater than 0, which indicates that the disorder of the system in the Cu^{2+} adsorption process was increased by the tested materials.

Isothermal adsorption and thermodynamic parameters of TC

Figure 8 shows the adsorption isotherm and adsorption rate of TC on the tested materials. The TC adsorption capacities of the materials increased with the increase in equilibrium concentration and were in accordance with the Langmuir model. Table 3 shows the Langmuir model fitting parameters for TC adsorption. The fitting of the TC adsorption isotherms of the test materials reached a very significant correlation level ($p < 0.01$). The q_m for TC adsorption changed from 118.60 to 602.83 mmol/kg, B/MBC had the best q_m for TC adsorption, and 50BS-B/MBC had the largest AR_e of 97.76%. Compared with the

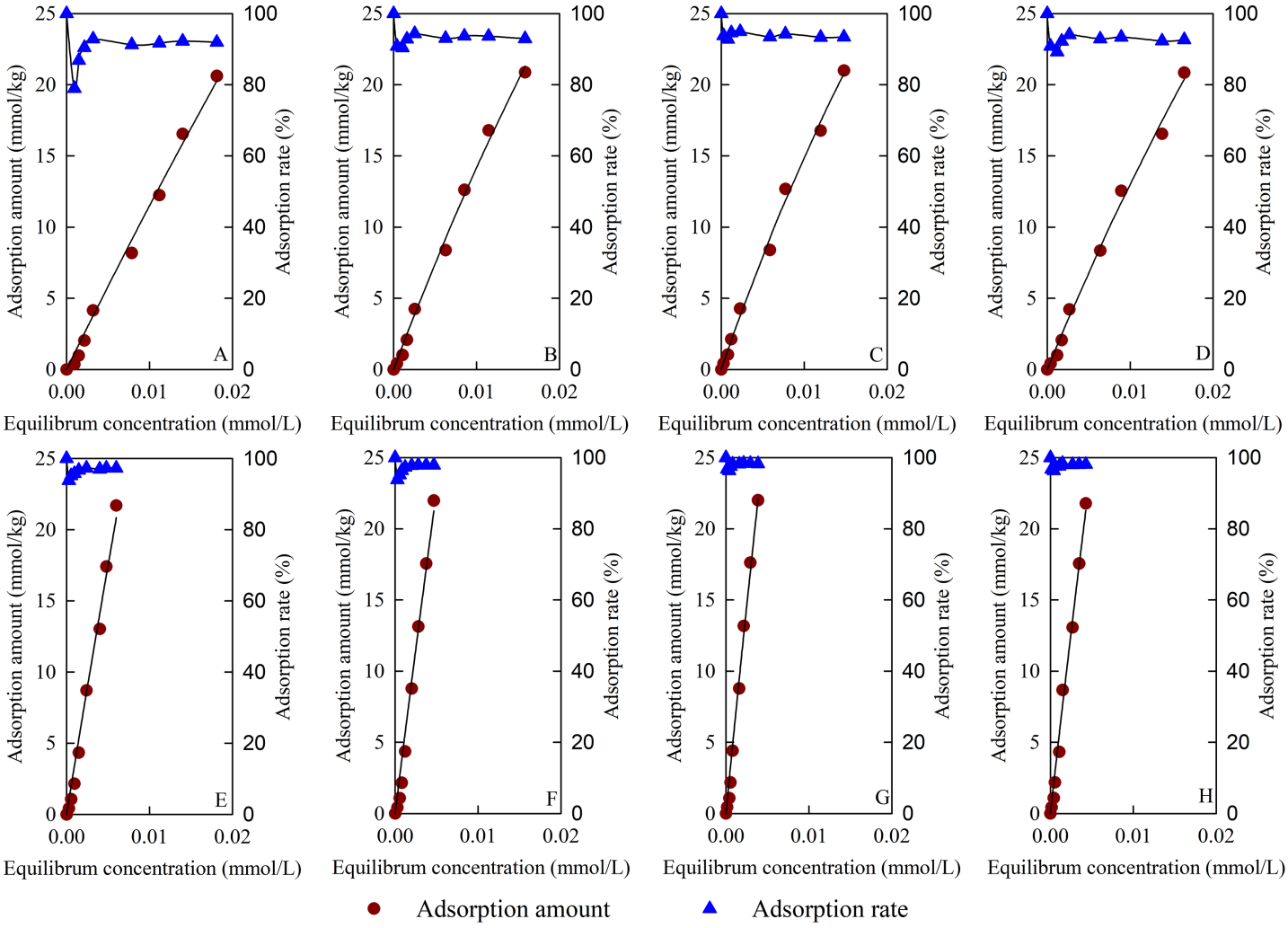

Figure 8 Adsorption isotherm and adsorption rate of TC. (A–H) BC, B/BC, 50BS-B/BC, 100BS-B/BC, MBC, B/MBC, 50BS-B/MBC, and 100BS-B/MBC, respectively.
Full-size DOI: 10.7717/peerj.13030/fig-8

Table 3 Langmuir fitting parameters and thermodynamic parameters for TC adsorption.

Treatments	Fitting parameters				Average adsorption rate (%)	Thermodynamic parameters			
	Correlation coefficient/r	Standard deviation/S	q_m (mmol/kg)	b		ΔG_{20} (kJ/mol)	ΔG_{40} (kJ/mol)	ΔH (kJ/mol)	ΔS (J/mol/K)
BC	0.9964**	0.70	336.59	3.53	89.54	−19.96	−21.34	0.41	69.47
B/BC	0.9975**	0.58	152.82	10.20	92.72	−22.49	−24.09	0.86	79.66
50BS-B/BC	0.9977**	0.56	118.60	14.30	93.83	−23.31	−24.96	0.92	82.63
100BS-B/BC	0.9971**	0.62	155.11	9.16	92.20	−22.23	−23.82	0.97	79.15
MBC	0.9945**	0.92	501.00	7.23	96.31	−21.67	−23.17	0.39	75.26
B/MBC	0.9919**	1.10	602.83	7.82	96.77	−21.81	−23.35	0.76	76.98
50BS-B/MBC	0.9955**	0.83	432.28	13.91	97.76	−23.24	−24.85	0.36	80.52
100BS-B/MBC	0.9953**	0.84	425.92	12.32	97.60	−22.91	−24.57	1.20	82.27

Note:
** The correlation coefficient is significant at $p = 0.01$ level ($r = 0.798$ when the degree of freedom $f = 7$ and the level of significance $p = 0.01$).

Table 4 Correlation s between Cu^{2+} (TC) adsorption and physicochemical properties. q_m and AR_e were maximum adsorption amount and average adsorption rate of Cu^{2+} (TC), respectively.

Adsorption parameters		Physicochemical properties	Regression equation	Correlation coefficients/*r*	Standard deviation/*S*
Cu^{2+}	q_m	pH	$pH = -0.01q_m + 10.01$	0.6039	0.44
		CEC	$CEC = 0.09q_m + 189.36$	0.0642	80.79
		S_{BET}	$S_{BET} = -0.06q_m + 22.38$	0.4696	5.74
	AR_e	pH	$pH = -2.22E + 10.62$	0.4895	0.49
		CEC	$CEC = 130.21E + 100.80$	0.1980	79.36
		S_{BET}	$S_{BET} = -27.25E + 33.72$	0.5156	5.57
TC	q_m	pH	$pH = 0.27q_m + 14.55$	0.2989	0.53
		CEC	$CEC = 6.02q_m + 79.86$	0.0459	80.87
		S_{BET}	$S_{BET} = 6.65q_m - 130.72$	0.6302	5.05
	AR_e	pH	$pH = -7.34E + 15.73$	0.4238	0.50
		CEC	$CEC = 56.66E + 154.80$	0.0225	80.94
		S_{BET}	$S_{BET} = 96.72E - 80.28$	0.4785	5.71

unmagnetized materials, the magnetized materials could reach the TC adsorption equilibrium quickly and had higher q_m values for TC adsorption. After B and BS-B loading, the *b* values of the materials for TC adsorption were larger than those of BC and MBC. At 20 and 40 °C, all test materials for TC adsorption had $\Delta G < 0$, which indicates that the adsorption was a spontaneous reaction; $\Delta H > 0$, which indicates that the adsorption was an endothermic reaction; and $\Delta S > 0$, which indicates that the disorder of the system increased in the TC adsorption process.

DISCUSSION

Correlation between adsorption and physicochemical properties

The q_m and AR_e values of each test material for Cu^{2+} and TC were linearly fitted to the physicochemical properties of the material, and the fitting results are shown in Table 4. CEC had positive correlations with the q_m and AR_e for Cu^{2+} and TC adsorptions; pH and S_{BET} had positive correlations with the q_m and AR_e for TC adsorption but had negative correlations with the q_m and AR_e for Cu^{2+} adsorption; pH had a negative correlation with the AR_e for TC adsorption. Moderate correlations between q_m and pH, and between AR_e and S_{BET} were observed in Cu^{2+} adsorption ($r > 0.5$); and the other indexes maintained a low degree of correlation. q_m and S_{BET} in TC adsorption were moderately correlated, and the other indexes maintained a low degree of correlation. The results indicate that the pH and S_{BET} of the material have a greater influence on Cu^{2+} and TC adsorptions respectively, than CEC.

Adsorption difference of Cu^{2+} and TC on BS-B/MBC

Figure 9 shows the adsorption difference of Cu^{2+} and TC on BS-B/MBC. The S_{BET}, pore structure, and functional groups of BC determined its adsorption capacity for Cu^{2+} and

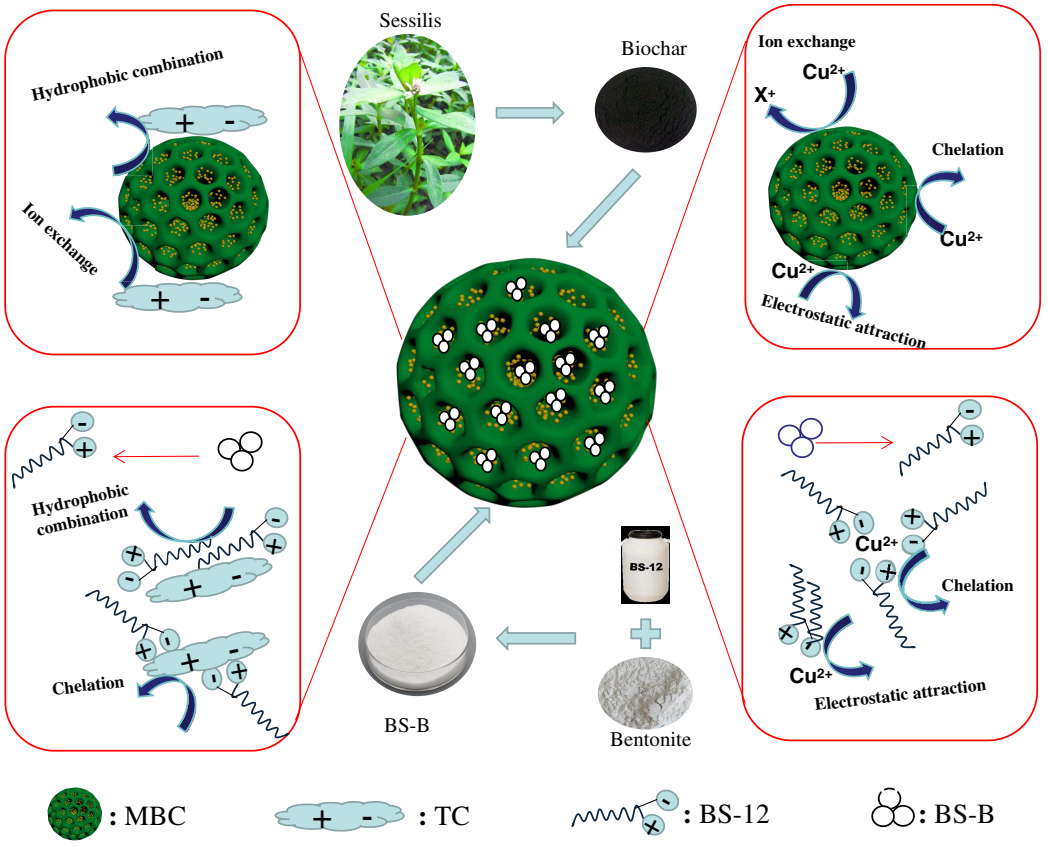

Figure 9 Adsorption differences of Cu^{2+} and TC on amphoteric-bentonite loaded magnetic-biochar. Full-size DOI: 10.7717/peerj.13030/fig-9

TC, but the adsorption capacity of original BC was limited. Solid–liquid separation could be realized under the action of external magnetic field by magnetizing the material with the magnetic medium. Fe_3O_4 loading increased the S_{BET} and effective adsorption sites on the surface of BC. MBC and BS-B/MBC had good magnetic separation performances and could be separated by applying a magnetic field.

B had strong adsorption capacity and ion exchange capacity, and amphoteric modification could remarkably improve its adsorption capacity for heavy metals and organic pollutants (*Li et al., 2016c*). Therefore, BS-B had high adsorption capacity for Cu^{2+} and TC. When MBC was loaded with BS-B, BS-B/MBC had a strong affinity for heavy metal ions and could effectively fix Cu^{2+}, and which increases the adsorption capacity for Cu^{2+}. The adsorption mechanism of Cu^{2+} comes from ion exchange, complexation, and electrostatic attraction by BC and from complexation and electrostatic attraction by BS-B (*Zhang et al., 2020*). TC has multiple ionizable functional groups, contains two groups of positive and negative charges, and has hydrophilicity (*Khanday & Hameed, 2018*). When the pH of the solution changed, the adsorption behavior of BS-B/MBC became more complicated. The relatively high surface area and large pore size of BS-B/

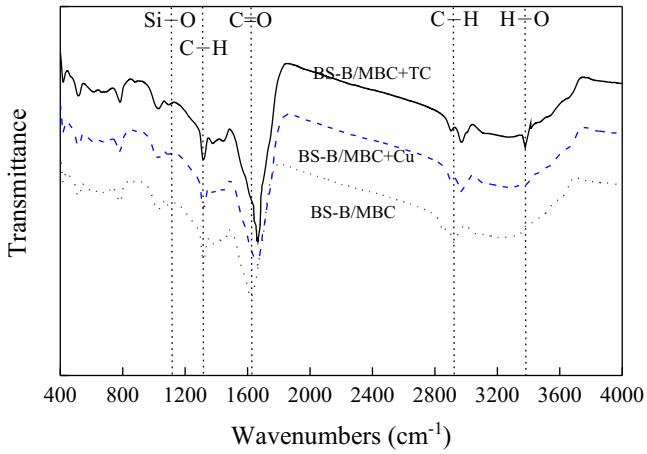

Figure 10 FTIR spectra of 100BS-B/MBC before and after Cu^{2+} and TC adsorption. 100BS-B/MBC +Cu and 100BS-B/MBC+TC were 100BS-B/MBC have absorbed Cu^{2+} and TC, respectively.
Full-size DOI: 10.7717/peerj.13030/fig-10

MBC provided more active sites for TC molecules (*Jang et al., 2018*). The rapid adsorption stage dominated the adsorption process of TC. The adsorption mechanism of TC comes from ion exchange and hydrophobic combination by BC and from complexation and hydrophobic combination by BS-B (*Zou et al., 2020*). Moreover, the FTIR spectra of 100BS-B/MBC before and after Cu^{2+} and TC adsorptions were compared (Fig. 10). The results showed that the C=O and C–H bonds on the surface of the material shifted after Cu^{2+} adsorption, which indicates that C=O and C–H on the surface of 100BS-B/MBC were involved in the Cu^{2+} and TC adsorption processes. The appearance of O–H bonds on 100BS-B/MBC after TC adsorption showed that hydroxyl group participates in the TC adsorption process. Additionally, the movement of the peak to a higher wave number means that the energy required for vibration is lower, which indicates that the group is more stable.

CONCLUSION

After magnetization, BC had reduced pH and CEC and increased S_{BET}. BC had a smooth surface, but the surface smoothness of BS-B/BC increased with the increase in BS-12 modification on BS-B. After Fe_3O_4 was loaded, a large number of Fe_3O_4 particles adhered to the surface of BS-B/MBC, and its surface became rough. Compared with unmagnetizatic ones, the magnetized materials had higher weight loss rates. FTIR and VSM analyses proved that BS-12 and Fe_3O_4 were modified to the surface of BS-B/MBC. MBC and BS-B/MC had good magnetic separation performances. BS-B/MBC had a good adsorption effects on Cu^{2+} and TC, and its AR_e was more than 80%. Cu^{2+} and TC adsorptions were spontaneous, endothermic, and entropy-adding reactions. The pH and S_{BET} of the material had a great influence on Cu^{2+} and TC adsorptions, respectively.

ADDITIONAL INFORMATION AND DECLARATIONS

Funding

This work was supported by the Fundamental Research Funds of China West Normal University (18B023), the Tianfu Scholar Program of Sichuan Province (2020-17), the Sichuan Province Science and Technology Support Program (2018JY0224) and the National Natural Science Foundation of P.R. China (41271244). The funders had no role in study design, data collection and analysis, decision to publish, or preparation of the manuscript.

Grant Disclosures

The following grant information was disclosed by the authors:
Fundamental Research Funds of China West Normal University: 18B023.
Tianfu Scholar Program of Sichuan Province: 2020-17.
Sichuan Province Science and Technology Support Program: 2018JY0224.
National Natural Science Foundation of P.R. China: 41271244.

Competing Interests

The authors declare that they have no competing interests.

Author Contributions

- Hongyan Deng performed the experiments, analyzed the data, prepared figures and/or tables, authored or reviewed drafts of the paper, and approved the final draft.
- Haixia He conceived and designed the experiments, performed the experiments, analyzed the data, prepared figures and/or tables, and approved the final draft.
- Wenbin Li conceived and designed the experiments, analyzed the data, authored or reviewed drafts of the paper, and approved the final draft.
- Touqeer Abbas conceived and designed the experiments, prepared figures and/or tables, and approved the final draft.
- Zhifeng Liu conceived and designed the experiments, analyzed the data, authored or reviewed drafts of the paper, and approved the final draft.

Data Availability

The following information was supplied regarding data availability:

The raw measurements are available in the Supplemental File.

Supplemental Information

Supplemental information for this article can be found online at http://dx.doi.org/10.7717/peerj.13030#supplemental-information.

REFERENCES

Ahmad M, Rajapaksha AU, Lim JE, Ming Z, Bolan N, Mohan D, Vithanage M, Sang SL, Yong SO. 2014. Biochar as a sorbent for contaminant management in soil and water: a review. *Chemosphere* **99(1)**:19–33 DOI 10.1016/j.chemosphere.2013.10.071.

Ana FV, Sérgio VPB, Ana C, Anabela C, Beatriz P. 2013. Influence of the storage conditions on the physicochemical properties, antioxidant activity and microbial flora of different tomato (*lycopersicon esculentum l.*) cultivars. *Journal of Agricultural Science* **5(2)**:118–128 DOI 10.5539/jas.v5n2p118.

Beraa A, Hajjaji M, Laurent R, Delavaux-Nicot B, Caminade AM. 2016. Removal of chromate from aqueous solutions by dendrimers-clay nanocomposites. *Desalination and Water Treatment* **57(30)**:14290–14303 DOI 10.1080/19443994.2015.1062429.

Feng LR, Jiao L, Yuan GD, Bi DX, Wei J. 2020. Biomass feedstocks and carbonization methods affect antibiotic adsorption on biochar. *China Environmental Science* **40(3)**:1156–1165 [in Chinese] DOI 10.19674/j.cnki.issn1000-6923.2020.0078.

Fu JG, Jia Y, Li Z, Huang YT, Wang XB, Zhao D. 2019. Preparation of Mg-Fe hydrotalcite supported on magnetic biochar and its adsorption capacity to Cd(II) and Ni(II) from water. *Environmental Protection of Chemical Industry* **39(5)**:574–580 [in Chinese] DOI 10.3969/j.issn.1006-1878.2019.05.015.

Garg R, Garg R, Thakur A, Arif SM. 2021. Water remediation using biosorbent obtained from agricultural and fruit waste. *Materials Today: Proceedings* **46(15)**:6669–6672 DOI 10.1016/j.matpr.2021.04.132.

He HX, Li WB, Deng HY, Ren LP, Li T. 2019. Surface characteristics of a recyclable and efficient adsorption material. *Materials Letters* **256**:126658 DOI 10.1016/j.matlet.2019.126658.

Isakovski MK, Beljin J, Trikovi J, Ronevi S, Maleti S. 2020. Current state and future perspectives of carbon based materials in the environment: fate and application. *Recent Patents on Nanotechnology* **15(3)**:183–196 DOI 10.2174/1872210514666201217150323.

Jang HM, Yoo S, Choi YK, Park S, Kan E. 2018. Adsorption isotherm, kinetic modeling and mechanism of tetracycline on Pinus taeda-derived activated biochar. *Bioresource Technology* **259(21)**:24–31 DOI 10.1016/j.biortech.2018.03.013.

Kastner JR, Mani S, Juneja A. 2015. Catalytic decomposition of tar using iron supported biochar. *Fuel Processing Technology* **130(9A)**:31–37 DOI 10.1016/j.fuproc.2014.09.038.

Khan F, Khan MJ, Samad A, Noor Y, Rashid M, Jan B. 2015. In-situ stabilization of heavy metals in agriculture soils irrigated with untreated wastewater. *Journal of Geochemical Exploration* **159(7)**:1–7 DOI 10.1016/j.gexplo.2015.07.002.

Khanday WA, Hameed BH. 2018. Zeolite-hydroxyapatite-activated oil palm ash composite for antibiotic tetracycline adsorption. *Fuel* **215(3)**:499–505 DOI 10.1016/j.fuel.2017.11.068.

Kumar L, Ragunathan V, Chugh M, Bharadvaja N. 2021. Nanomaterials for remediation of contaminants: a review. *Environmental Chemistry Letters* **19(6)**:3139–3163 DOI 10.1007/s10311-021-01212-z.

Kyung-Won J, Brian HC, Tae-Un J, Kyu-Hong A. 2016. Facile synthesis of magnetic biochar/ Fe_3O_4 nanocomposites using electro-magnetization technique and its application on the removal of acid orange 7 from aqueous media. *Bioresource Technology* **220**:672–676 DOI 10.1016/j.biortech.2016.09.035.

Lawal AA, Hassan MA, Farid M, Yasim-Anuar T, Shirai Y. 2021. Adsorption mechanism and effectiveness of phenol and tannic acid removal by biochar produced from oil palm frond using steam pyrolysis. *Environmental Pollution* **269(15)**:116197–116208 DOI 10.1016/j.envpol.2020.116197.

Li G, Zhu W, Zhang C, Shen Z, Zhao W. 2016a. Effect of a magnetic field on the adsorptive removal of methylene blue onto wheat straw biochar. *Bioresource Technology* **206**:16–22 DOI 10.1016/j.biortech.2015.12.087.

Li WB, Meng ZF, Liu Z, Chen HY, Wu Q, Xu SE. 2016b. Chromium (VI) adsorption characteristics of bentonite under different modification patterns. *Polish Journal of Environmental Studies* **25(3)**:1075–1083 DOI 10.15244/pjoes/61626.

Li WB, Liu Z, Meng ZF, Ren S, Xu SE, Zhang Y, Wang MY. 2016c. Composite modification mechanism of cationic modifier to amphoteric modified kaolin and its effects on surface characteristics. *International Journal of Environmental Science and Technology* **13(11)**:2639–2648 DOI 10.1007/s13762-016-1091-3.

Li WB, He HX, Kang L, Yang DQ, Zhuang Q, Meng ZF, Li XL, Li YX. 2020. Restoration of Cu^{2+}-contaminated purple soil by applying yeasract and interplant. *Applied Ecology and Environmental Research* **18(5)**:6623–6635 DOI 10.15666/aeer/1805_66236635.

Lopez J, Boyd D, Ylitalo GM, Littnan C, Pearce R. 2012. Persistent organic pollutants in the endangered Hawaiian monk seal (*Monachus schauinslandi*) from the main Hawaiian Islands. *Marine Pollution Bulletin* **64(11)**:2588–2598 DOI 10.1016/j.marpolbul.2012.07.012.

Mazurkiewicz J, Mazur A, Mazur R, Chmielowski K, Janczak D. 2020. The process of microbiological remediation of the polluted Słoneczko reservoir in Poland: for reduction of water pollution and nutrients management. *Water* **12(11)**:3002–3011 DOI 10.3390/w12113002.

Meng ZF, Zhang YP, Wang GD. 2007. Sorption of heavy metal and organic pollutants on modified soils. *Pedosphere* **17(2)**:235–245 DOI 10.1016/S1002-0160(07)60030-7.

Min Z, Liu YS, Zhao JL, Liu WR, He LY, Zhang JN, Chen J, He LK, Zhang QQ, Ying GG. 2018. Occurrence, fate and mass loadings of antibiotics in two swine wastewater treatment systems. *Science of the Total Environment* **639(6)**:1421–1431 DOI 10.1016/j.scitotenv.2018.05.230.

Mohan D, Sarswat A, Ok YS, Pittman CU. 2014. Organic and inorganic contaminants removal from water with biochar, a renewable, low cost and sustainable adsorbent: a critical review. *Bioresource Technology* **160(1)**:191–202 DOI 10.1016/j.biortech.2014.01.120.

Nyamukamba P, Moloto MJ, Tavengwa N, Ejidike IP. 2019. Evaluating physicochemical parameters, heavy metals, and antibiotics in the influents and final effluents of South African wastewater treatment plants. *Polish Journal of Environmental Studies* **28(3)**:1305–1312 DOI 10.15244/pjoes/85122.

Park JH, Ok YS, Kim SH, Cho JS, Heo JS, Delaune RD, Dong-Cheol S. 2016. Competitive adsorption of heavy metals onto sesame straw biochar in aqueous solutions. *Chemosphere* **142(1)**:77–83 DOI 10.1016/j.chemosphere.2015.05.093.

Said AEA, Goda MN. 2021. Superior competitive adsorption capacity of natural bentonite in the efficient removal of basic dyes from aqueous solutions. *Chemistry Select* **6(11)**:2790–2803 DOI 10.1002/slct.202100575.

Shah LA, Silva-Valenzuela MDGD, Farooq M, Khattak SA, Diaz V, Rolando F. 2018. Influence of preparation methods on textural properties of purified bentonite. *Applied Clay Science* **162(9)**:155–164 DOI 10.1016/j.clay.2018.06.001.

Wang B, Li Y, Zheng J, Hu Y, Wang X, Hu B. 2020. Efficient removal of U(VI) from aqueous solutions using the magnetic biochar derived from the biomass of a bloom-forming cyanobacterium (*Microcystis aeruginosa*). *Chemosphere* **254**:126898–126909 DOI 10.1016/j.chemosphere.2020.126898.

Xin O, Han Y, Xi C, Chen J. 2017. Magnetic biochar combining adsorption and separation recycle for removal of chromium in aqueous solution. *Water Science & Technology* **75(5)**:1177–1184 DOI 10.2166/wst.2016.610.

Yan J, Han L, Gao W, Xue S, Chen M. 2015. Biochar supported nanoscale zerovalent iron composite used as persulfate activator for removing trichloroethylene. *Bioresource Technology* **175**:269–274 DOI 10.1016/j.biortech.2014.10.103.

Yang X, Liu JJ, Mcgrouther K, Huang HG, Lu KP, Guo X, He LZ, Lin XM, Che L, Ye ZQ, Wang HL. 2016. Effect of biochar on the extractability of heavy metals (Cd, Cu, Pb, and Zn) and enzyme activity in soil. *Environmental Science and Pollution Research* **23(2)**:974–984 DOI 10.1007/s11356-015-4233-0.

Zhao YH, Li WB, Yi HY, Liang Q, Dong ZM, Deng HY. 2021. Adsorption and desorption mechanisms of Cu^{2+} on amended subsurface riverbank soils. *Desalination and Water Treatment* **221(5)**:252–259 DOI 10.5004/dwt.2021.27045.

Zhang YF, Deng HY, Zhu L, Xie J, Kang L, Li WB, Liu W, Meng ZF. 2020. Difference of adding different compositely modified amphipathic maifanite on Cu^{2+} adsorption. *Desalination and Water Treatment* **178(2)**:203–210 DOI 10.5004/dwt.2020.24968.

Zou Y, Deng HY, Li M, Zhao YH, Li WB. 2020. Enhancing tetracycline adsorption by riverbank soils by application of biochar-based composite materials. *Desalination and Water Treatment* **207(2)**:332–340 DOI 10.5004/dwt.2020.26392.

Zulfiqar M, Sufian S, Bahadar A, Lashari N, Mansor N. 2021. Surface-fluorination of TiO_2 photocatalysts for remediation of water pollution: a review. *Journal of Cleaner Production* **317(5)**:128354–128365 DOI 10.1016/j.jclepro.2021.128354.